

1

Visible Light Positioning and Its Integration with Visible Light Communication

Chen Chen and Zhihong Zeng

Contents

Introduction	2
Integrated VLCP Using FBMC-SCM and PDOA	2
Principle	
Performance of Communication and Positioning	
Integrated VLCP with Adaptive Transmission	7
Principle	
Performance of Communication and Positioning	Ç
Conclusion.	15
References	14

Abstract

Visible light communications (VLC) and visible light positioning (VLP) are two promising supplementary technologies for 6G and Internet of Things (IoT) networks. To simultaneously support communication and positioning capabilities, visible light communications and positioning (VLCP) can be seamlessly integrated within the same system using illumination LED lamps and photodetectors (PDs). In this chapter, two integrated VLCP systems are discussed, including an integrated VLCP system using filter bank multicarrier-based subcarrier multiplexing (FBMC-SCM) and phase difference of arrival (PDOA) and an advanced integrated VLCP system with adaptive transmission.

C. Chen $(\boxtimes) \cdot Z$. Zeng

Chongqing University, Chongqing, China

e-mail: c.chen@cqu.edu.cn

Keywords

Visible light positioning · Visible light communication · Integrated visible light communication and positioning

Introduction

The globally wide-spread LED lamps for illumination purposes provide functional devices for not only signal modulations but also imaginations of novel wireless communication and positioning approaches. Compared with radio frequency (RF) systems, visible light generated by illumination LED lamps has negligible influence on sensitive electronic equipment. Hence, visible-light-based systems are compatible with scenarios like aircraft, hospital, airport, underwater, and underground which require communication and positioning facilities with stability concerns. In recent years, both visible light communications (VLC) and visible light positioning (VLP) have been widely investigated in the past two decades [1–4]. Although individual VLC and VLP systems have their own unique advantages, the integration of visible light communications and positioning (VLCP) for simultaneous communication and positioning has been further proposed and investigated [5–9]. To enable the seamless integration of VLC and VLP, the joint communication and positioning signal design and the efficient signal transmission are two key challengers to be addressed for practical implementation of integrated VLCP systems.

In this chapter, two integrated VLCP systems are discussed in detail, including an integrated VLCP system using filter bank multicarrier-based subcarrier multiplexing (FBMC-SCM) and phase difference of arrival (PDOA) [10, 11] and an advanced integrated VLCP system with adaptive transmission [12].

Integrated VLCP Using FBMC-SCM and PDOA

In practical indoor environments, a number of LED lamps are usually installed to set up a VLC system to satisfy lighting requirements and to provide data communication and estimate the location of an indoor user. The LED lamps generally use the intensity modulation with direct detection (IM/DD), where the intensity of each LED lamp is modulated with the transmitted data and a photodetector (PD) is used to convert the light into an electrical signal. In the integrated VLCP system, two-dimensional (2D) PDOA-based positioning is applied at the receiver to estimate the locations of indoor users [13].

Principle

The block diagram of the integrated VLCP system is shown in Fig. 1, where three LED lamps are adopted at the transmitter side and one PD is used at the receiver

side. To implement the PDOA-based positioning, three LED lamps are synchronized and modulated with four sinusoidal signals with four different frequencies, where f_1 and f_4 are both modulated to LED 1, while f_2 and f_3 are modulated to LED 2 and LED 3, respectively. Let d_i be the distance between the i-th (i = 1, 2, 3) LED lamp and the PD. It has been shown in [13] that there exists the position shifting effect in practical PDOA-based VLP systems caused by the nonuniform initial time delay pattern of the commercial off-the-shelf LEDs, which can be efficiently mitigated by the neural-network-based post-compensation approach. At the receiver, the differential PDOA algorithm is executed and finally two distance differences, i.e., d_1 – d_2 and d_2 – d_3 , can be obtained. Given the locations of the three LED lamps and the distance differences, the position of the user can be successfully estimated. The detailed procedures to implement PDOA-based positioning can be found in [13].

Insets (a) and (b) in Fig. 1 present the principle of modulation and demodulation of OFDM/FBMC, respectively. In order to reduce the large OOBI, FBMC applies a prototype filter to filter each subcarrier. The principles of the two modulation schemes are the same, except that the CP insertion in OFDM is replaced by the polyphaser network (PPN)-based filtering in FBMC [14]. As shown in Fig. 1a, after quadrature amplitude modulation (QAM) mapping, Hermitian symmetry is imposed before the inverse fast Fourier transform (IFFT) so as to generate a real-valued signal. To guarantee the orthogonality between adjacent subcarriers, offset QAM (OQAM) with a half-symbol-duration offset is applied [14]. For the generation of FBMC signals, the Mirabbasi-Martin filter (MM filter) is applied [15].

As can be seen from Fig. 1, the total modulation bandwidth of the integrated VLCP system is divided into three subbands with two GBs. Specifically, subbands 1 and 3 are used for VLC, while subband 2 is reserved for PDOA positioning. In addition, the two GBs are assumed to have the same frequency spacing. It should be noted that all the LED lamps are used to transmit the same OFDM/FBMC-encoded communication signal which is carried by subbands 1 and 3. By adopting such a transmit diversity transmission scheme, the implementation complexity can

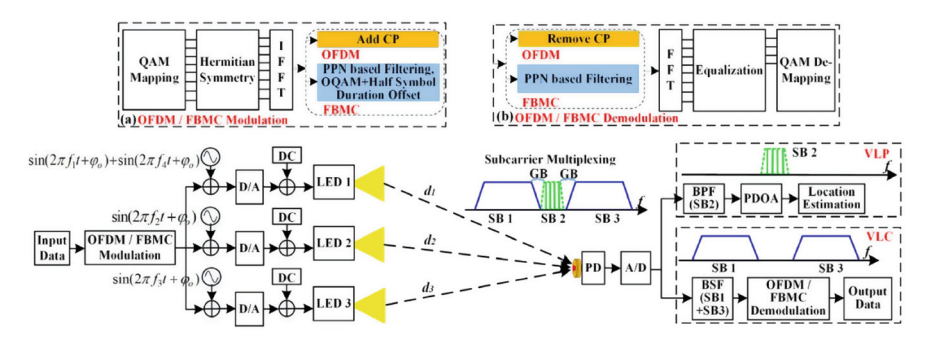


Fig. 1 Block diagram of the integrated VLCP system. Insets: principle of OFDM/FBMC (a) modulation and (b) demodulation

be reduced compared with our previous scheme in [10]. Before digital-to-analog conversion (D/A), the sinusoidal signals for VLP and the OFDM/FBMC signal for VLC are added together with respect to each LED lamp. Subsequently, direct current (DC) biases are added and the resultant signals are utilized to drive the three LED lamps, respectively. The sinusoidal signals for VLP are synchronized at the transmitter. At the receiver side, the optical signal is detected by the PD and converted into an electrical signal. On one hand, subband 2 which contains the positioning signal can be obtained by using a BPF, and the location of the user can be calculated according to the PDOA algorithm [13]. On the other hand, subbands 1 and 3 containing the communication signal can be achieved with a band-stop filter (BSF), and OFDM/FBMC demodulation is then applied to recover the communication data. Hence, both the communications and positioning purposes can be achieved in this integrated VLCP system.

Performance of Communication and Positioning

The feasibility of the integrated VLCP system within a practical indoor environment is verified via the following experimental results. The experimental setup of the integrated VLCP system is depicted in Fig. 2. Both the OFDM/FBMC signal for

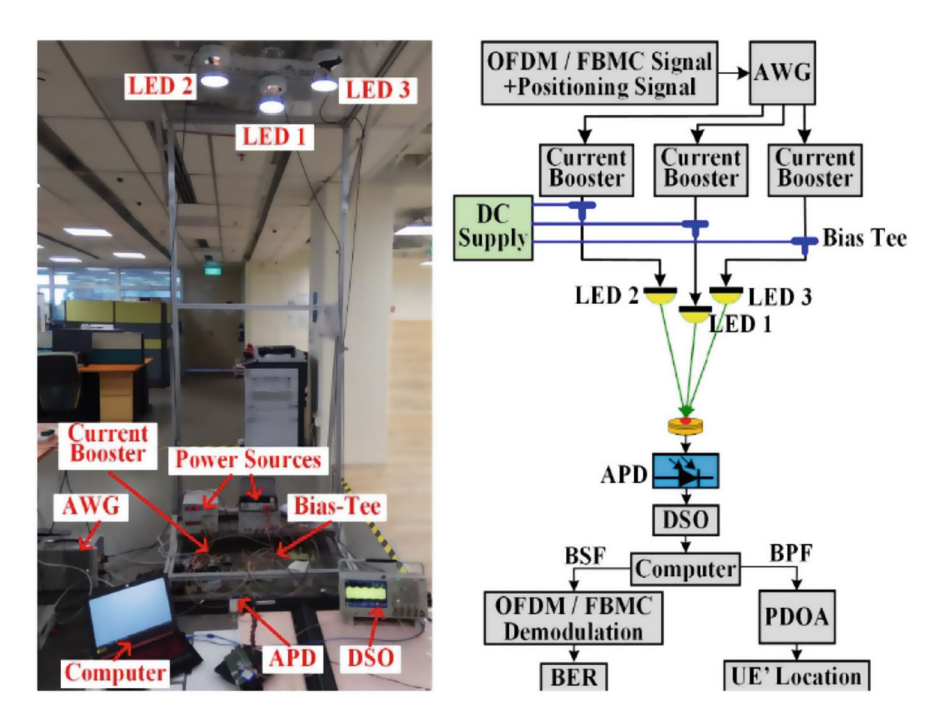


Fig. 2 Experimental setup of the integrated VLCP system

VLC and the sinusoidal signals for VLP are offline generated using MALTAB, which are then uploaded to a multichannel arbitrary waveform generator (AWG, Spectrum M4x. 6622-x4) with a sampling rate of 100 MSa/s. After amplifying and adding DC biases, the obtained signals are used to drive three LED lamps (Lumileds LXML-PWCI). After free-space propagation, the light is captured by an avalanche PD (APD, Hamamatsu S8664-50K) after passing by a blue filter (BF). The detected signal is recorded by a digital storage oscilloscope (Tektronix MDO3104) with a sampling rate of 100 MSa/s. Subsequently, the demodulation of the communication signal and the estimation of the user's location are executed offline using MALTAB. To extend the modulation bandwidth, digital pre-frequency domain equalization is used in the system [16]. The performance of the integrated VLCP system is tested in a quarter area of 1.2×1.2 m, and the vertical distance between the LED lamps and the PD is 2.1 m. The locations of three LED lamps are (0, -0.175, 2.1), (0.25, -0.175, 2.1)0.075, 2.1), and (-0.25, 0.075, 2.1) with the origin (0, 0, 0), where the units are all meters. The APD has an active area of 19.6 mm² and a responsivity of 15 A/W at the wavelength of 450 nm. The system modulation bandwidth is extended to 10 MHz, and 4-QAM mapping is used for communication. For both OFDM and FBMC, the IFFT/FFT size is 512, and the number of data subcarriers is 51. The overlapping factor in FBMC is set to K = 4. The frequencies of the four sinusoidal signals for positioning are in the range between 5.1 and 5.7 MHz with a frequency gap of 0.2 MHz. Figure 3a and b shows the received electrical spectra of the OFDM-SCM signal and the FBMC-SCM signal, respectively, where the GB spacing is 0.7 MHz. It can be seen that, compared with OFDM, the OOBI of FBMC is effectively suppressed, resulting in much reduced power leakage at the positioning frequency subband. A significant 6-dB OOBI reduction can be achieved by using FBMC-SCM in comparison to OFDM-SCM.

Figure 4a and b demonstrates the positioning results over the testing area in the integrated VLCP system using FBMC-SCM and OFDM-SCM, respectively. The

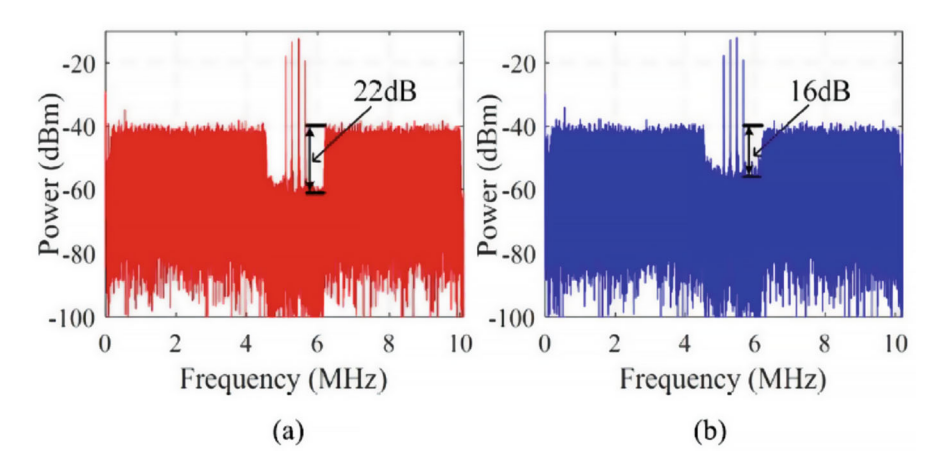


Fig. 3 Received spectra of (a) FBMC-SCM signal and (b) OFDM-SCM signal

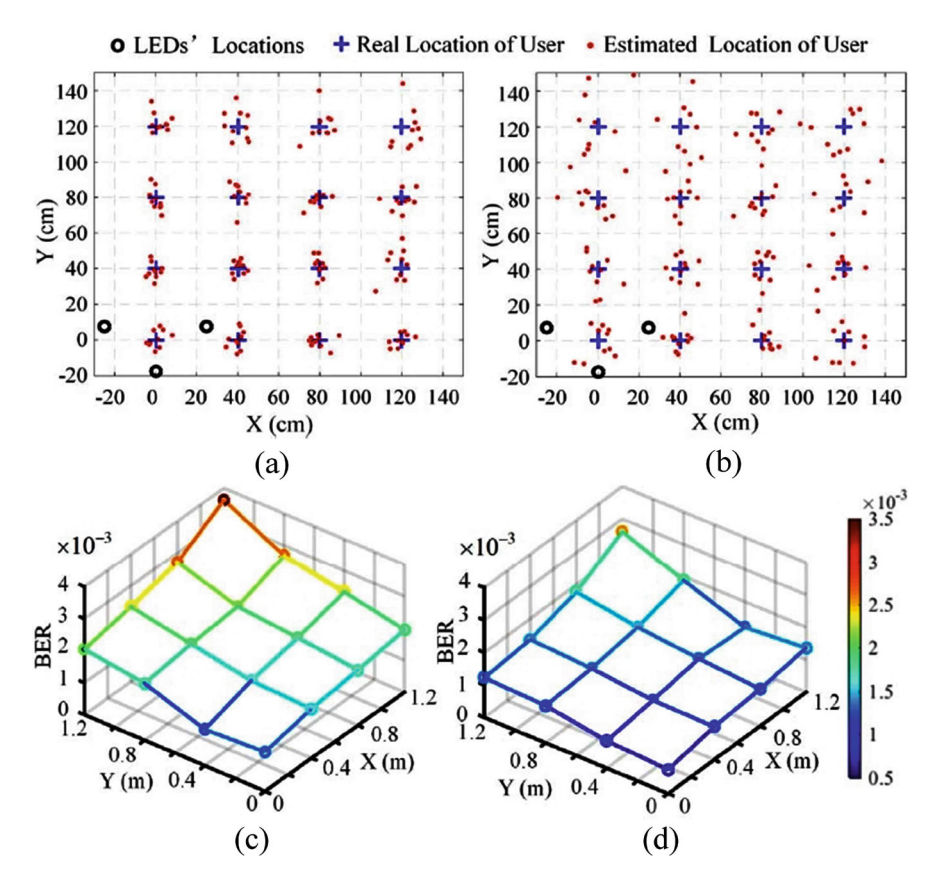


Fig. 4 Positioning results based on (a) FBMC-SCM and (b) OFDM-SCM, and BER distribution of (c) FBMC-SCM and (d) OFDM-SCM

frequency spacing of GB is set to 0.7 MHz. As can be seen, when the user is moving away from the LED lamps, the positioning accuracy is gradually deceased for both FBMC-SCM and OFDM-SCM. It can be clearly observed that a higher positioning accuracy is achieved by using FBMC-SCM compared with OFDM-SCM over the 1.2×1.2 m coverage area. For FBMC-SCM, most of the positioning errors are less than 8 cm, and only a few of them are more than 10 cm when the user is at edge of the coverage area, and the mean position error is 6.08 cm. However, for OFDM-SCM, the positioning errors are mainly ranging from 7 to 20 cm, and only a few of them are below 5 cm when the user is at center of the coverage area, and the mean positioning error is as high as 10.91 cm. Moreover, Fig. 4c and d shows the BER distribution over the testing area using OFDM-SCM and FBMC-SCM, respectively. It can be seen that the BER values over the testing area for both OFDM-SCM and FBMC-SCM are all less than 3.8×10^{-3} . More specifically, due to the adverse effect of

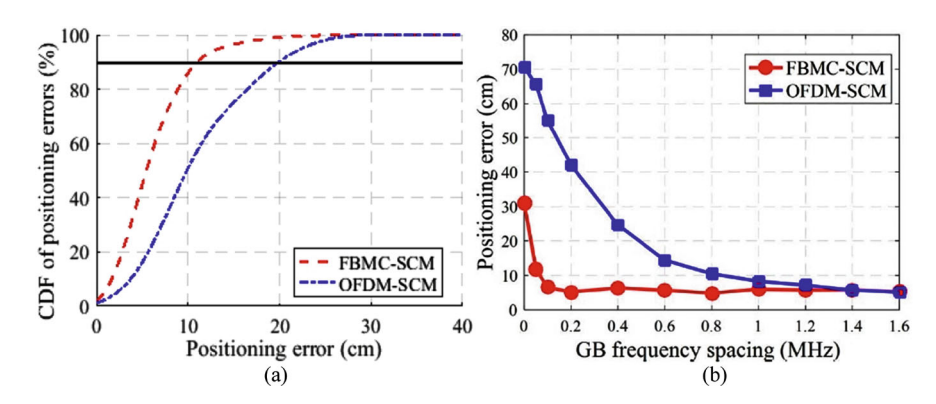


Fig. 5 Positioning results: (a) CDF of positioning errors using OFDM-SCM and FBMC-SCM, and (b) positioning error versus GB frequency spacing

subcarrier filtering in FBMC [15], the BER performance of FBMC-SCM is slightly worse than that of OFDM-SCM but still remains at a comparable level.

Figure 5a shows the cumulative distribution functions (CDFs) of the positioning errors using OFDM-SCM and FBMC-SCM. As can be seen, the positioning errors at 90% confidence for OFDM-SCM and FBMC-SCM are 19.6 and 11.2 cm, respectively, which indicates a positioning accuracy improvement of up to 8.4 cm. Figure 5b presents the positioning error versus the GB frequency spacing. For OFDM-SCM, the positioning error is gradually reduced as the GB frequency spacing is increased from 0 to 1.4 MHz. However, a rapid reduction of positioning error is shown for FBMC-SCM when the GB frequency spacing is increased from 0 to 0.1 MHz. It can be observed that OFDM-SCM achieves nearly the same positioning accuracy as the FBMC-SCM only when the GB frequency spacing is larger than 1.4 MHz. To achieve the best positioning accuracy, OFDM-SCM requires a minimum GB frequency spacing of 1.4 MHz; however, FBMC-SCM only requires a negligible GB frequency spacing of 0.1 MHz. Defining the effective bandwidth utilization ratio (EBUR) as the ratio of the bandwidth occupied by the communication and positioning signals to the total modulation bandwidth, the EBURs using OFDM-SCM and FBMC-SCM to achieve the same positioning accuracy are 72% and 98%, respectively.

Integrated VLCP with Adaptive Transmission

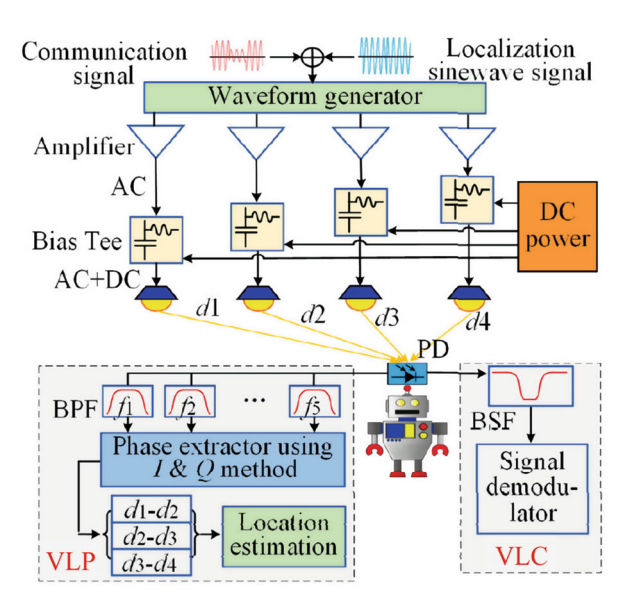
To enhance the performance of the integrated VLCP systems, adaptive transmission has been further designed for the integrated VLCP systems, where an advanced differential phase difference of arrival (A-DPDOA) positioning algorithm is also developed to simplify hardware complexity and improve tracking robustness [12].

Principle

The system architecture of the integrated VLCP with adaptive transmission is provided in Fig. 6. At the transmitter side, communication signals and synchronized positioning sinewave signals are initially generated from a signal generator, i.e., arbitrary waveform generator. The integrated communication and positioning signals are first amplified and then combined with DC biases by bias-tees to drive the corresponding LED lamps. At the mobile device side, the receiver consists of an APD with an integrated electrical amplifier, a VLC module, and a VLP module. After receiving the optical signals from the LED lamps, the APD converts the optical signal into electrical signals and then captures them by using an oscilloscope. The Raspberry Pi is used to perform communication signal demodulation, power measurement, and location estimation. After receiving the mixed integrated communication and positioning signals from four LED lamps, band-pass filters (BPFs) and band-stop filter (BSF) are applied to filter both the positioning signal and communication signal out from the received mixed signal, respectively. For positioning, A-DPDOA is proposed to estimate the location of devices, as it can simplify hardware without using LOs and it is robust against background noise and random tilting of PD plane in real-world settings [12].

In the integrated VLCP system, K devices (e.g., robot, machine, and phone) randomly distribute on the floor. The system has a central controller, which connects all LEDs to transmit signal to devices. Once the central controller collects the feedback information (e,g., channel information and devices' services), it can schedule the communication and positioning tasks. The bandwidth is equally divided into N subcarriers. As each LED lamp has one unique positioning subcarrier to transmit

Fig. 6 The system model of the integrated VLCP with adaptive transmission



positioning sinusoidal signal, expect one of them having two unique positioning subcarriers in our proposed positioning algorithm, totally L+1 subcarriers out of the N subcarriers are applied for localization, while the N-L-1 subcarriers are used for communication. As the system has K devices, there have K communication subcarrier groups (SGs). The power allocation trade-off between VLC and VLP, and the interference (OOBI) will affect each other. When the transmission power of LED is fixed, if the VLCP system allocates more power to VLC spectrum subcarriers, the system can achieve the higher communication data rate, but the positioning subcarriers will be allocated with less power and the positioning accuracy will decrease in this case. In contrast, if the system allocates more power on positioning subcarriers, the positioning accuracy can be improved due to the high received signal strength, but the communication data rate will decline due to the less received signal power. Thus, there exists some trade-off between them in terms of power allocation. In order to enhance the performance of the integrated VLCP systems, a joint adaptive modulation, subcarrier allocation, and power allocation are presented to improve the localization accuracy and communication performance. The detailed adaptive transmission design can be found in [12].

Performance of Communication and Positioning

The experimental setup is illustrated in Fig. 7a, which is configured with a coverage area of $222.5 \,\mathrm{m}^3$. The locations of four LEDs are (-0.4, 0.4, 1.35), (0.4, 0.4, 1.35), (-0.4, 0.4, 1.35), and <math>(-0.4, -0.4, 1.35) in meters. The Inverse Fast Fourier Transform (IFFT) size N=256. The modulation bandwidth is $20 \,\mathrm{MHz}$. The modulation order $M=\{2,4,8,16,32,64\}$ and $BER_{max}=3.8\times10^{-3}$. The frequencies of the five sinusoidal signals for localization range from 4.0 to 4.8 MHz with each frequency gap being $0.2 \,\mathrm{MHz}$. Generally, the 2D localization service of the proposed localization needs at least three LED lamps, and the 3D localization

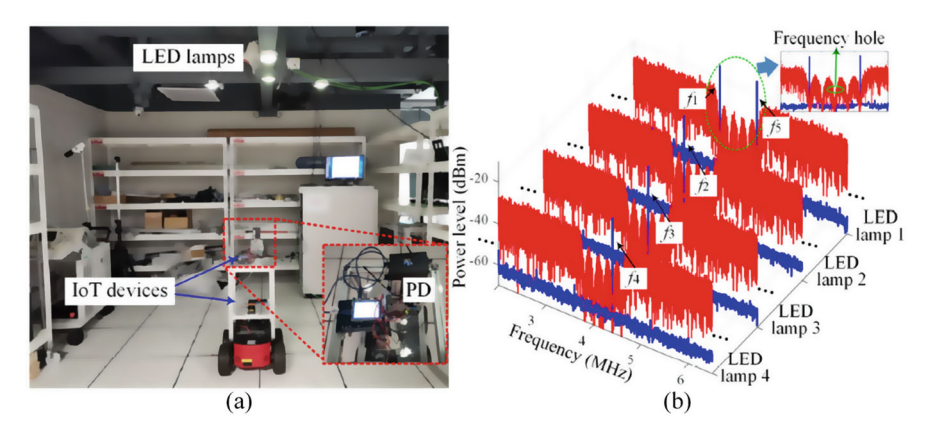


Fig. 7 (a) Experimental setup and (b) electrical spectra of the integrated signal

service of the proposed localization needs at least four LED lamps. Generally, the 2D localization service of the proposed localization scheme needs at least three LED lamps, and the 3D localization service of the proposed localization scheme needs at least four LED lamps. In the manuscript, as an experimental setup, four LED lamps are used to demonstrate the performance. The PD equipped with each device is put at the top of the robot or indoor vehicle.

Figure 7b shows the electrical spectra of integrated communication and positioning signals at the LED transmitter sides. Both the communication signal and positioning sinewave signal are generated by using MATLAB tool, and they are respectively allocated on the communication subcarriers and positioning subcarriers. Then, these two kinds of signal are added together at the LED transmitter side. For the positioning module, the sinusoidal signals with five different frequencies (blue color), i.e., from f_1 to f_5 , are modulated on the four LED lamps. LED lamp 1 carries two sinusoidal signals with frequencies f_1 and f_5 , while LED lamp 2, LED lamp 3, and LED lamp 4 use frequencies f_2 , f_3 , and f_4 to transmit sinusoidal signals, respectively. Note that these five frequencies are not used to transmit communication signals in one unit of the VLCP system. From Fig. 7b, it can be seen that there are five frequency holes in the identified subcarriers that have negligible OOBI leakage from adjacent communication subcarriers (red color). In the context, the localization sinusoidal signals (blue color) are put into these frequency holes, to avoid the interference leakage on localization frequency holes from the communication signals. Figure 8a shows the CDF of the 2D positioning error distributions, where it is found that when the vertical height is 1.5 m, the positioning errors are less than 10 cm in 90%. The CDF of 3D positioning errors is provided in Fig. 8b, where the localization errors are less than 20 cm in 90% at the height of 1.5 m. These results verify the high localization accuracy of A-DPDOA in both 2D and 3D localization environments.

The positioning robustness of the proposed A-DPDOA-based positioning and the existing RSS-based positioning is evaluated [17]. As shown in Fig. 9, the PD plane

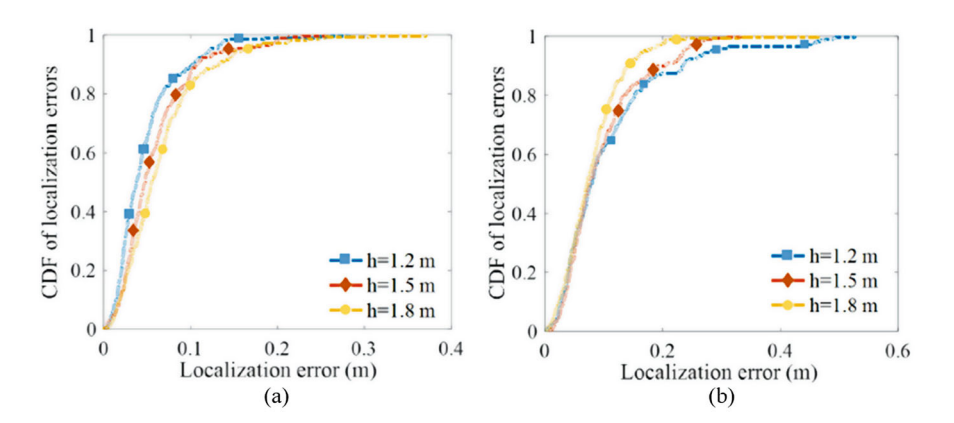
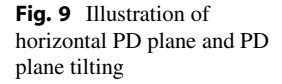
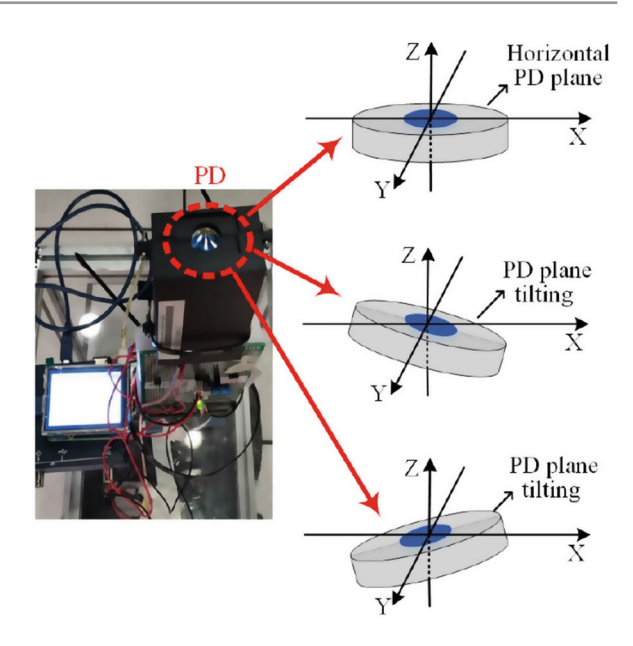


Fig. 8 CDF of positioning errors: (a) 2D positioning and (b) 3D positioning





can maintain at a horizontal level when the indoor ground is absolutely smooth. However, when some areas of the indoor ground are uneven, the PD plane tilts to a certain degree which decreases the receiver signal strength transmitted from some LED lamps, and finally degrades the positioning performance.

As illustrated in Fig. 10, two tests each of eight measurements at one fixed location at the coordinate (0.4, 2, 1.5 m) are conducted with PD plane tilting, where the measurements of A-DPDOA distance difference and received RSS amplitude are provided in this figure. Note that the first four measurements are under the normal condition with the PD plane being horizontal, while the next four measurements are under PD plane tilting. The PD plane tilting randomly ranges from 10 degree to 20 degree in these measurements. It can be easily observed that both A-DPDOA and RSS measurements are affected by the random tilting of PD plane, and RSS measurements are more sensitive to PD plane tilting than that of A-DPDOA. For example, the received RSS amplitude significantly changes from 40 millivolt (mV) of horizontal PD plane to about 20 mV of PD plane tilting, while the distance difference of A-DPDOA only changes from 2.6 to 2.7 m during this process. Figure 10 also illustrates the positioning results of the proposed A-DPDOA-based positioning and the existing RSS-based positioning under PD plane tilting. The blue dots and black dots show the normal measurements under horizontal PD plane of A-DPDOA and RSS, respectively, the dark red dots present the positioning results of A-DPDOA under PD plane tilting, and the blue dots show the positioning results of RSS under PD plane tilting. As can be seen, the estimated locations (dark red dots) of A-DPDOA are very close to the actual locations in the presence of PD plane tilting, while the estimated locations (blue dots) of RSS deviate from the actual 12 C. Chen and Z. Zeng

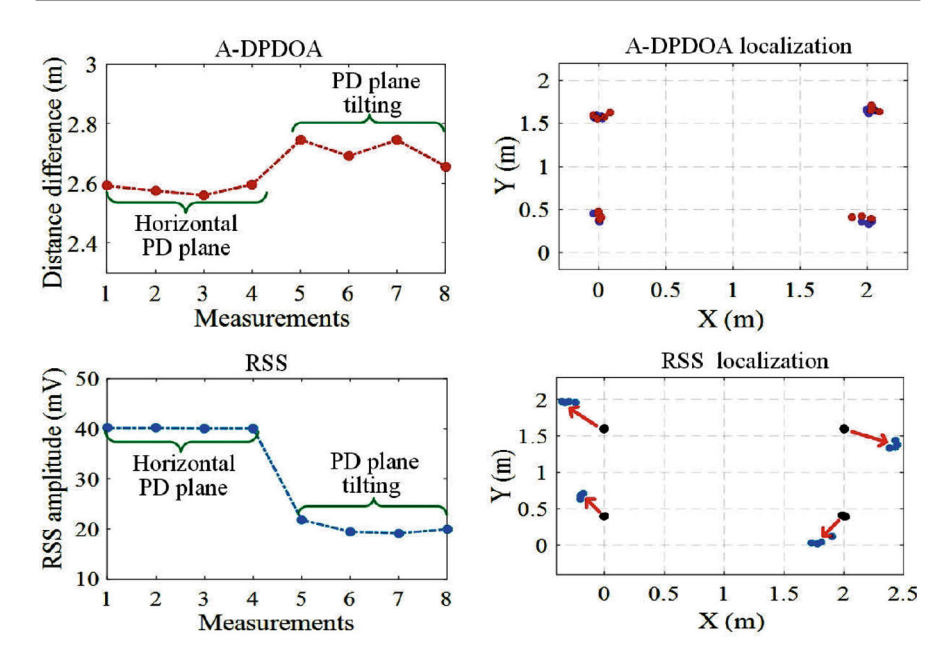


Fig. 10 Measurements under random tilting of PD plane

locations in this case. The reason lies in the fact that when the PD plane tilts, the current measurements of the received signal power from all LED lamps deviate from the actual measurements, where the RSS utilizes the measured received power strength to perform localization which is relatively sensitive to the PD plane tilting, while A-DPDOA measures the phase difference between LED lamps and the PD instead of received power strength which is less sensitive to PD plane tilting. The experimental results have verified that the proposed A-DPDOA-based positioning can obtain higher robustness than that of the RSS-based positioning against PD plane tilting.

Figure 11 illustrates the total transmission data rate of all devices and the QoS satisfaction level under different input current levels for the three schemes. When the input current increases, both the system data rate and the QoS satisfaction performance are improved due to the increased received signal power at devices. Our proposed joint optimization scheme (joint power allocation, subcarrier allocation, and adaptive modulation) outperforms the joint weighted preequalization and modulation scheme, because the system optimizes subcarrier allocation. By contract, the joint preequalization and modulation scheme achieves the worse data rate performance, the reason is that it has low bandwidth utilization as the bandwidth is divided into several independent subbands for four LEDs, and it needs some number of subcarriers as guard bands to avoid OOBI. From Fig. 11b, the results verify that the proposed adaptive transmission scheme efficiently satisfies the QoS requirements of devices.

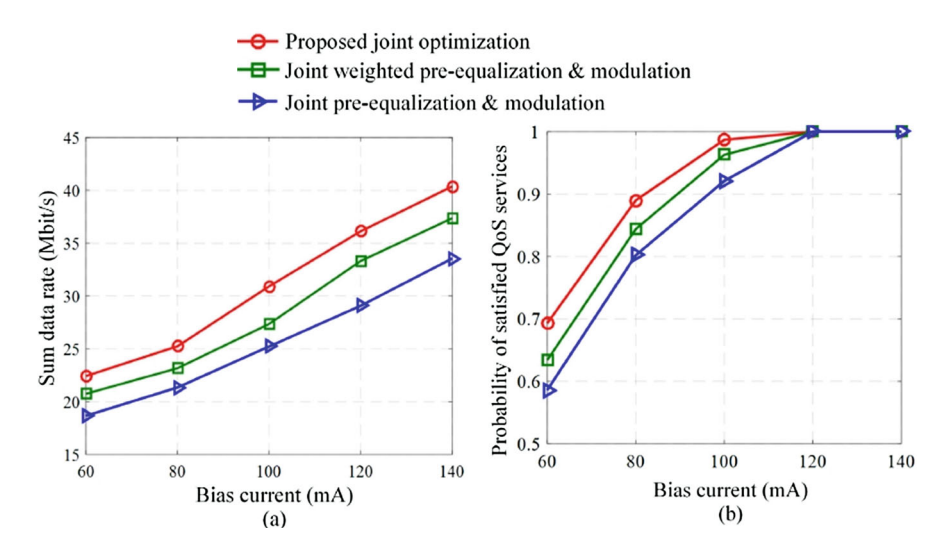
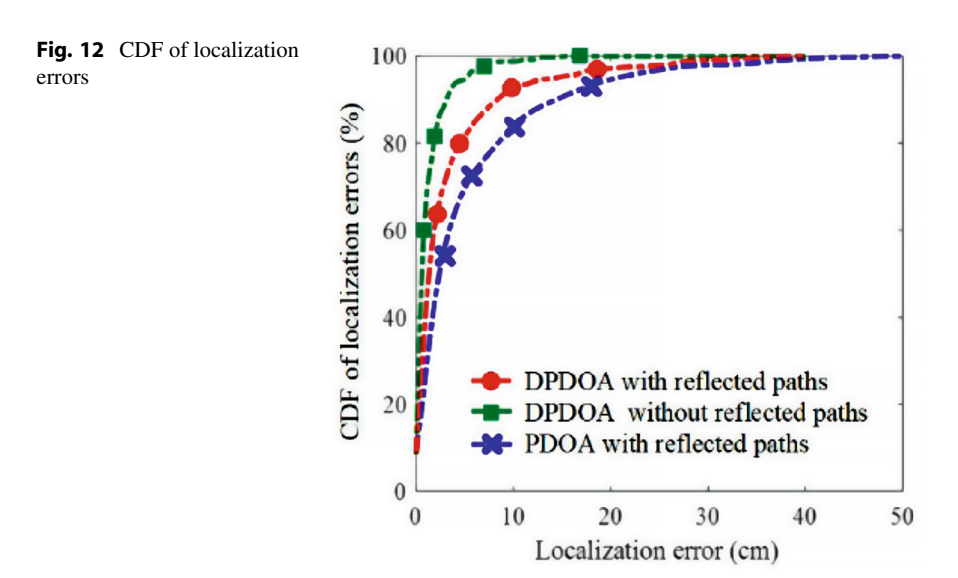


Fig. 11 (a) Sum transmission data rate and (b) the QoS satisfaction level under different bias currents (mA)



Here, simulations are provided to evaluate the effect of the reflected paths on the positioning performance of our proposed system over the $3\times3\,\mathrm{m}^2$ coverage area, and the positioning performance between DPDOA and PDOA is compared. As shown in Fig. 12, the positioning accuracy will decrease due to the negative effect of

the reflected paths. However, for PDOA, the positioning errors are mainly ranging from 5 to 10 cm, and the positioning error is higher than 20 cm when the device locates near the room edge, and the mean positioning error is as high as 8.04 cm. Compared with PDOA, DPDOA does not need the help of LOs and thus can avoid the negative effect on LOs of both system setup and positioning accuracy.

Figure 13 illustrates the effect of the power allocation trade-off value on the integrated VLCP system with the communication and positioning performances when the total bias current is 140 mA and the localization error threshold is 8 cm. Note that the transmit power is determined by the bias current at transmitters. When the trade-off value α is 0.4, the probability for localization errors within 8 cm is 82.4% and the achievable data rate is 22.3 Mbps. From Fig. 13, it can also be observed that as the increase of α , the more power will be allocated for communication and thus the data rate enhances during this process. However, as the power allocated for positioning decreases, the positioning error increases (positioning accuracy reduces) accordingly. It is worth noting that when the trade-off value α changes from 0.6 to 0.7, the probability for localization errors within 8 cm significantly decreases from 57.2% to 36.3%. This phenomenon indicates that the positioning error is super big when the power allocated for positioning is less than $0.4 \times P_{tot}$. In addition, it is also found that the communication data rate decreases when α changes from 0.4 to 0.3.

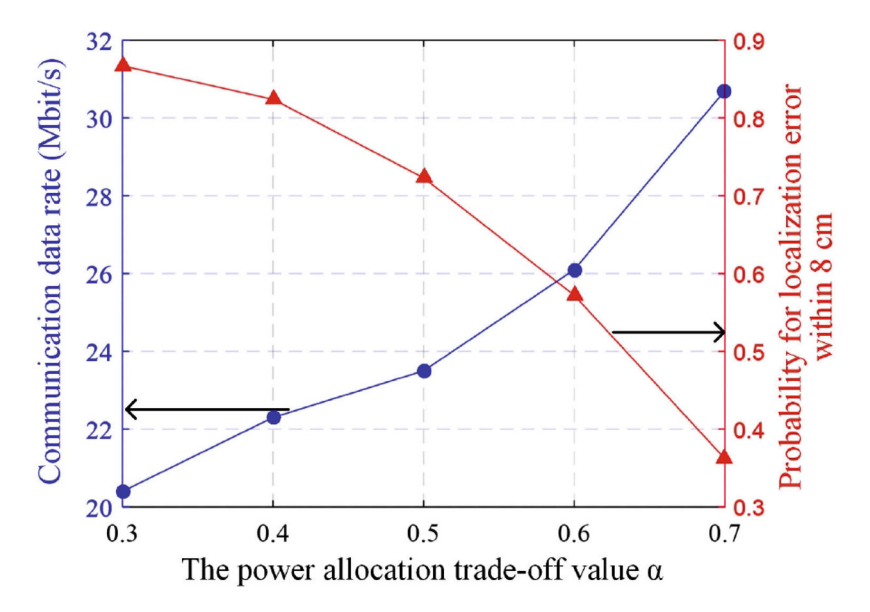


Fig. 13 The impact of the power allocation trade-off value on communication and positioning performances

Conclusion

In this chapter, an integrated VLCP system using FBMC-SCM and PDOA is first discussed, where the use of FBMC-SCM can significantly reduce the power leakage when compared with OFDM-SCM and hence a negligible GB frequency spacing of 0.1 MHz is required. Moreover, an advanced integrated VLCP system with adaptive transmission is further reported, where hardware complexity simplification and tracking robustness improvement are achieved by utilizing the A-DPDOA positioning algorithm. Therefore, efficient integration of both communication and positioning functions using light can be a promising technology for practical application in various indoor scenarios.

Competing Interest Declaration The author(s) has no competing interests to declare that are relevant to the content of this manuscript.

References

- Komine T, Nakagawa M (2004) Fundamental analysis for visible-light communication system using LED lights. IEEE Trans Consum Electron 50:100–107
- Chi N, Zhou Y, Wei Y et al (2020) Visible light communication in 6G: Advances, challenges, and prospects. IEEE Veh Technol Mag 15:93–102
- Armstrong J, Sekercioglu Y, Neild A (2013) Visible light positioning: a roadmap for international standardization. IEEE Commun Mag 51:68–73
- 4. Luo J, Fan L, Li H (2017) Indoor positioning systems based on visible light communication: state of the art. IEEE Commun Surv Tutor 19:2871–2893
- 5. Chen J, You X (2017) Visible light positioning and communication cooperative systems. In: International Conference on Optical Communications and Networks (ICOCN), pp 1–3
- Yang H, Du P, Zhong W et al (2019) Reinforcement learning-based intelligent resource allocation for integrated VLCP systems. IEEE Wirel Commun Lett 8:1204–1207
- 7. Yang H, Zhong W, Chen C et al (2020) Integration of visible light communication and positioning within 5G networks for Internet of things. IEEE Netw 34:134–140
- Yang H, Zhong W, Chen C et al (2020) Coordinated resource allocation-based integrated visible light communication and positioning systems for indoor IoT. IEEE Trans Wirel Commun 19:4671–4684
- Yang H, Zhong W, Chen C et al (2020) QoS-driven optimized design-based integrated visible light communication and positioning for indoor IoT networks. IEEE Internet Things J 7:269– 283
- Yang H, Chen C, Zhong W et al (2010) An integrated indoor visible light communication and positioning system based on FBMC-SCM. In: IEEE Photonics Conference (IPC), pp 129–130
- 11. Yang H, Chen C, Zhong W et al (2018) Demonstration of a quasi-gapless integrated visible light communication and positioning system. IEEE Photon Technol Lett 30:2001–2004
- Yang H, Zhang S, Alphones A (2023) An advanced integrated visible light communication and localization system. IEEE Trans Commun 71:7149–7162
- 13. Zhang S, Zhong W, Du P et al (2018) Experimental demonstration of indoor sub-decimeter accuracy VLP system using differential PDOA. IEEE Photon Technol Lett 30:1703–1706
- Jung S, Kwon D, Yang S, Han S (2016) Inter-cell interference mitigation in multi-cellular visible light communications. Opt Express 24:8512–8526

16 C. Chen and Z. Zeng

15. Bellanger M, Le Ruyet D, Roviras D et al (2010) FBMC physical layer: a primer. PHYDYAS 25:7–10

- Chen C, Zhong W, Wu D (2016) Indoor OFDM visible light communications employing adaptive digital pre-frequency domain equalization. In: Conference on Lasers and Electro-Optics (CLEO), JTh2A.118
- 17. Amini C, Azmi P, Kashef S (2021) An accurate ranging algorithm based on received signal strength in visible light communication. J Lightwave Technol 39:4654–4660